IOPscience iopscience.iop.org

Home Search Collections Journals About Contact us My IOPscience

Spectral electron momentum density calculation in graphite

This article has been downloaded from IOPscience. Please scroll down to see the full text article.

1995 J. Phys.: Condens. Matter 7 3895

(http://iopscience.iop.org/0953-8984/7/20/009)

View the table of contents for this issue, or go to the journal homepage for more

Download details:
IP Address: 171.66.16.151
The article was downloaded on 12/05/2010 at 21:19

Please note that terms and conditions apply.

J. Phys.: Condens. Matter 7 (1995) 3895–3904. Printed in the UK

Spectral electron momentum density calculation in graphite

A S Kheifets and M Vos

Electronic Structure of Materials Centre, The Flinders University of South Australia, GPO Box 2100, Adelaide 5001, Australia

Received 13 February 1995

Abstract. The linear muffin tin orbital method has been used to calculate the energy–momentum distribution of valence electrons in graphite along major symmetry directions and as the spherical average over the irreducible wedge of the Brillouin zone. These data bridge the gap between existing band structure calculations and the emerging electron momentum spectroscopy of solids. The calculation has been validated by comparison to the most accurate experimental data on highly oriented laser-annealed carbon films.

1. Introduction

The electronic band structure of graphite has been studied thoroughly by both theory and experiment. Band energies at high-symmetry points have been found from angle-resolved photoemission measurements and confirmed by density functional calculations within an accuracy of 1 eV (see Charlier *et al* (1991) and references therein). Band energies are obtained from the density functional calculations as eigenvalues of the Kohn–Sham equations (Kohn and Sham 1965). The eigenfunctions, i.e. the wave functions of electrons, can also be calculated and are generally much more sensitive to the computation scheme details. However, unlike the band energies, the wave functions cannot be measured directly in experiment. With the advent and recent development of electron momentum spectroscopy on solids a new way of testing electron wave functions has become possible. It is known that, under the independent particle approximation, the spectral electron momentum density (SEMD) is proportional to the modulus squared of the one-electron wave function in momentum space. The SEMD gives the probability of finding an electron within unit range of energy and momentum and can be measured directly by the coincidence electron momentum spectroscopy based on the (e, 2e) reaction (McCarthy and Weigold 1988, 1991).

Graphite was the first solid state target used to study valence band electron energy–momentum distribution by the (e, 2e) technique (Gao *et al* 1988). The experimental SEMD was compared with a density functional calculation based on the mixed basis pseudopotential approach. A good agreement was found between the measurement and calculation. However, the significance of this result was diminished by rather poor energy and momentum resolutions (8.6 eV and 0.25–0.40 au, respectively). Subsequently, the SEMD was measured with a considerably improved resolution (1.5 eV and 0.15 au) on amorphous graphite (Kheifets *et al* 1994). The linear muffin tin orbital (LMTO) method based on the density functional theory was used to obtain the spherically averaged SEMD which described correctly dispersion of the two major peaks on the experimental spectra. However, the spectra contained also some additional features which did not follow the calculation and could be attributed to the amorphous nature of the target. Another (e, 2e)

0953-8984/95/203895+10$19.50 © 1995 IOP Publishing Ltd

study was performed on highly oriented pyrolytic graphite (HOPG) (Vos *et al* 1994). This is a polycrystalline material with all microcrystals aligned in the c direction while their in-plane orientation is chaotic. The SEMD was probed for momenta directed perpendicular to the c axis. The LMTO calculation with spherical averaging in the basal plane was used to interpret the experimental results. The experimental spectra contained some unexpected features. However, the dispersion and intensity of the main free-electron-like peak were described quite accurately.

Despite improving the energy resolution and the quality of the samples, the test of electron wave functions in graphite using the (e, 2e) technique is far from complete. On the theoretical side, graphite is the ultimate challenge for the LMTO method which is designed for closely packed solids whose elementary cell can be spanned effectively by touching atomic spheres. The elementary cell of graphite is abnormally stretched along the c axis. It prevents straightforward application of the LMTO method.

The purpose of this paper is to get very accurate LMTO results on the band structure and the SEMD of graphite to provide a reference for (e, 2e) studies on both oriented and polycrystalline targets. We demonstrate that the LMTO method is applicable to graphite when a sufficient number of empty muffin tin (MT) spheres is added to the elementary cell. We show that significant improvement is achieved on the previous LMTO calculations (Kheifets *et al* 1994, Vos *et al* 1994) where no empty spheres were used.

2. Theory

We employ the LMTO method as described in the monograph of Skriver (1984). In this method the atomic polyhedron is substituted with a number of atomic spheres each of which represents a non-equivalent atomic position. The graphite elementary cell has four carbon atom positions belonging to the two widely separated layers:

layer I	$(0, 0, -c/4)$	$(0, a/\sqrt{3}, -c/4)$
layer II	$(0, 0, c/4)$	$(a/2, a/2\sqrt{3}, c/4)$

where a and c are the two major lattice parameters. The graphite structure has a very loose packing with the ratio $c/a = 1.66\,(c/a)_0$, where for the ideal close-packed structure (HCP) $(c/a)_0 = \sqrt{8/3}$.

This creates a difficulty in direct application of the LMTO method because the electron potential becomes discontinuous over the elementary cell. The problem, however, can be effectively overcome if several fictitious 'empty' MT spheres are inserted into the cell (Glötzel *et al* 1980). We chose the following high-symmetry positions for the empty spheres:

layer 0	$(0, 0, 0)$
layer Ia	$(0, 0, -c/2)$

The equivalent position at layer IIa, $(0, 0, c/2)$, can be reached by a primitive vector translation and is not included in the MT basis.

Since the elementary cell of graphite is stretched along the c axis and the empty MT spheres have to span the cell in this direction we chose the MT radius of the empty spheres R_e to be larger than the radius R_C of the spheres placed at the carbon atom cites. The total volume of the MT spheres has to be equal to the volume of the elementary cell:

$$N_C \tfrac{4}{3}\pi R_C^3 + N_e \tfrac{4}{3}\pi R_e^3 = a^2 c\sqrt{3}/2. \tag{1}$$

This equation leaves one of the radii, R_C or R_e, free to choose and we use it as an adjustable parameter to get the best fit of the band energies at high-symmetry points. Using this

procedure we obtain $R_C = 1.800$ au and $R_e = 2.546$ au. These values satisfy equation (1) with the lattice parameters $a = 4.641$ au, $c = 12.654$ au (2.456 Å and 6.696 Å, respectively, according to Wyckoff (1963)) and $N_C = 4$, $N_e = 2$. Here and throughout atomic units are used.

The one-electron wave function within any particular sphere centred at r_s can be written as

$$\psi_{jk}(r - r_s) = \sum_{lm} a_{slm}^{jk} \mathrm{i}^l Y_{lm}(r_1) \frac{1}{r_1} P_{sl}(r_1) \qquad r_1 = |r - r_s| \leqslant R_s. \tag{2}$$

Here k is the crystal wave vector, j is the band index, Y_{lm} are the spherical harmonics depending on the orbital momentum l and its projection m. The expansion coefficients a_{slm}^{jk} for a given MT sphere s are found by solving the LMTO eigenvalue problem.

Table 1. Characteristic valence band energies (in eV) of graphite evaluated from the Fermi level.

	LMTO		Other theoretical		Experimental	
	a	b	c	d	e	f
Bottom σ	−20.1	−20.4	−20.1	−20.6	−20.6	
	−17.9	−19.5	−19.8	−20.4		
Bottom π	−11.9	−8.8	−8.9	−9.0	−8.1	−8.5
	−7.6	−6.7	−6.8	−6.9	−7.2	−6.6
Top σ	−5.1	−4.0	−3.5	−3.3	−4.6	−5.5
Unoccupied σ	9.4	5.2	3.7	3.6		

[a] Kheifets *et al* (1994).
[b] Present work.
[c] Gao *et al* (1988).
[d] Charlier *et al* (1991).
[e] Eberhardt *et al* (1990).
[f] Law *et al* (1983).

By definition, the SEMD is expressed through the Fourier transform of the one-electron wave function ψ_{jk}:

$$\rho_j(\epsilon, q) = (2\pi)^{-3} \sum_{Gk} n_{jk} \left| \int \mathrm{d}^3 r \, \psi_{jk}(r) \mathrm{e}^{-\mathrm{i}q\cdot r} \right|^2 \delta_{q,k+G} \, \delta(\epsilon - E_j(k)) \qquad k \in \text{1st BZ}. \tag{3}$$

Here n_{jk} and E_{jk} are the occupation number and energy of the corresponding one-electron state. The integration in equation (3) is carried out over the unit cell where the wave function ψ_{jk} is normalized to unity. The reciprocal lattice vector G translates the momentum q to the first Brillouin zone (BZ). The SEMD is normalized over energy and momentum space to the number of valence electrons per unit cell per spin:

$$2 \sum_j \int \mathrm{d}\epsilon \, \mathrm{d}q \, \rho_j(\epsilon, q) = N_e. \tag{4}$$

The SEMD can be integrated over momentum or energy which gives either the density of states

$$2 \sum_j \int \mathrm{d}q \, \rho_j(\epsilon, q) = N(\epsilon) \tag{5}$$

or the energy-integrated electron momentum density (EMD)

$$\int \mathrm{d}\epsilon\, \rho_j(\epsilon, q) = \rho_j(q). \tag{6}$$

Taking advantage of the central field expansion (2) the SEMD can be readily calculated as

$$\rho_j(\epsilon, q) = \frac{2}{\pi} \sum_{Gk} n_{jk} \left| \sum_s \mathrm{e}^{-\mathrm{i}q\cdot r_s} \sum_{lm} a_{slm}^{jk} Y_{lm}(k) \int_0^{R_s} \mathrm{d}r\; j_l(qr) P_{sl}(r) \right|^2 \delta_{q,k+G}\, \delta(\epsilon - E_j(k)) \tag{7}$$

where $j_l(qr)$ is the spherical Bessel function. The expansion coefficients a_{slm}^{jk} and the one-electron energies $E_j(k)$ are found by solving the LMTO eigenvalue problem. An equivalent expression for the EMD $\rho_j(q)$ is similar to equation (7) but does not contain the δ function of energy.

We will be concerned with momentum densities along certain high-symmetry directions in the momentum space. In this case the SEMD, $\rho_j(\epsilon, q)$, $q = qe$, becomes a function of only two scalar variables, ϵ and q, and can be presented conveniently as a set of energy profiles at various momenta. The EMD $\rho_j(qe)$ becomes a function of one scalar variable q and can be plotted alongside with the energy bands when the extended zone scheme is used.

When analysing the (e, 2e) data on a polycrystalline target the spherically averaged momentum densities are essential. They can be obtained by integration over the irreducible wedge of the BZ. For the graphite structure the averaged SEMD is obtained as

$$\rho_j(\epsilon, q) = (4\pi)^{-1} \int \mathrm{d}\Omega_q\, \rho_j(\epsilon, q) = \frac{3}{\pi} \int_0^1 \mathrm{d}\sin\vartheta_q \int_0^{\pi/6} \mathrm{d}\varphi_q\, \rho_j(\epsilon, q). \tag{8}$$

For analysing the (e, 2e) experiments on HOPG-type materials only the polar integration in equation (8) is required.

3. Numerical results

We present the calculated band energies at high-symmetry points in table 1 along with other theoretical and experimental results. As we mentioned above, we use the MT radii as adjustable parameters to get the best fit of the band energies. As one can see from the table our energies are very close to other experimental and calculated values. By using different size empty muffin tin spheres we achieved a considerable improvement on the previous LMTO results of Kheifets *et al* (1994) where no empty MT spheres were used.

In figure 1 we plot the band energies $E_j(q)$ and the EMD $\rho_j(q)$, $q = qe$, as functions of q along the three major high-symmetry directions ΓK, ΓM and ΓA (columns 1–3, respectively). The same momentum scale is used in both band energy (upper row) and momentum density (lower row) plots. Where the momentum q extends beyond the first BZ a reciprocal lattice vector translation pulls it back as indicated in equation (3).

Because of the quasi-two-dimensional structure, energy bands in graphite can be classified as σ and π according to their transformation under reflection with respect to the basal plane. The three σ bands (σ_1, σ_2 and σ_3) originate from the hybridized s–p_x–p_y atomic orbitals whereas the atomic p_z orbital gives rise to the π band. Weak interaction between the carbon layers doubles each band with a very small separation of the two resulting subbands.

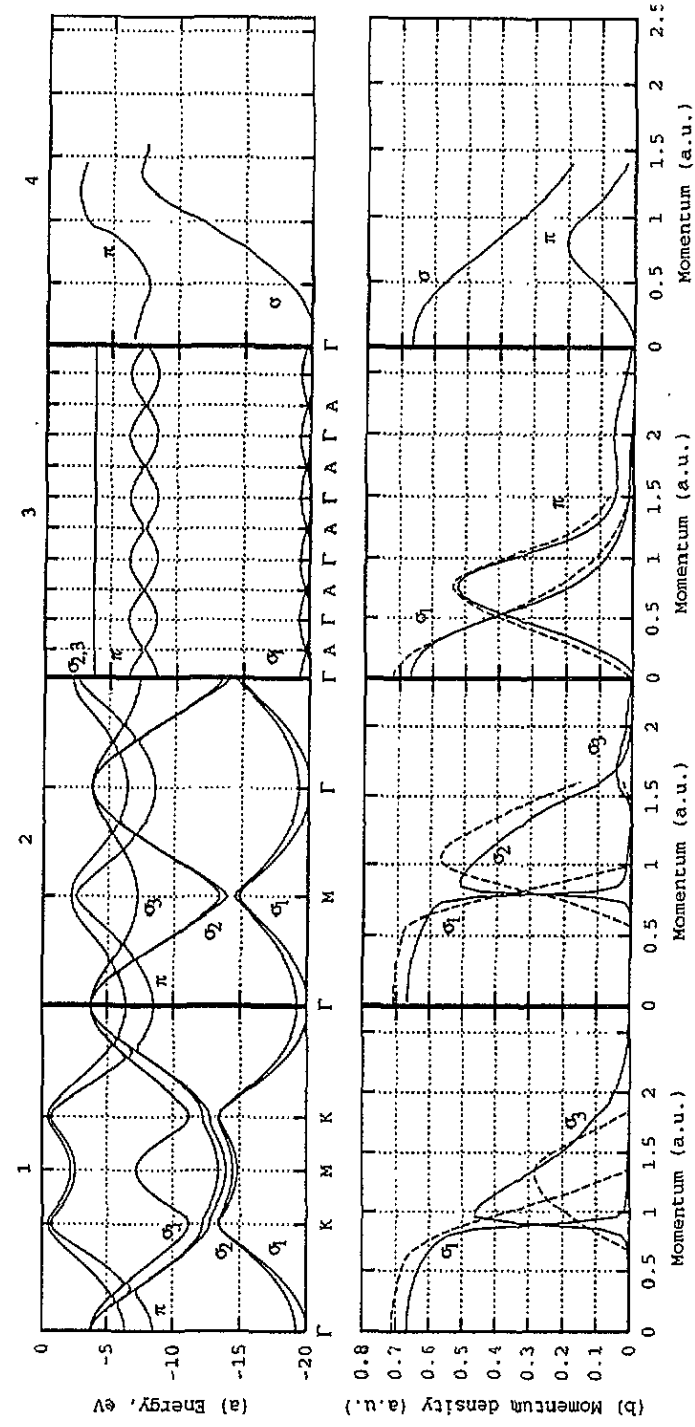

Figure 1. Energy bands relative to the Fermi level (a) and electron momentum densities (b) in ΓK, ΓM and ΓA directions (1–3) and as the spherical average (4). Solid lines—present calculation, dashed lines—results from Gao *et al* (1988).

For the two in-plane directions, ΓK and ΓM, only σ bands contribute to the EMD. The π bands give zero contribution as the corresponding wave functions are odd with respect to the reflection while the exponential factor $\exp(-i\boldsymbol{q}\cdot\boldsymbol{r})$ remains unchanged under this transformation. For the out-of-plane ΓA direction both σ and π bands contribute to the momentum density.

In the same figure 1 we also present the EMD calculations of Gao *et al* (1988) obtained within a mixed basis pseudopotential approach. Although the two sets of curves are generally similar, there is a noticeable difference in magnitude, especially in the σ band contribution in the ΓK and ΓM directions. This is despite the fact that the band energies are quite close in both calculations as follows from table 1. This shows that momentum densities, calculated through the one-electron wave functions, are much more sensitive to the computation scheme details than the band energies.

From the two plots, the band energies $E_j(q)$ and the EMD $\rho_j(q)$, it is possible to reconstruct the SEMD $\rho_j(\epsilon, q)$ as a function of energy and momentum $q = qe$ in a certain direction. In the ΓK direction the SEMD disperses along the band σ_1 and then switches gradually to σ_3 thus following almost continuously a free-electron-like parabola up to the middle of the second BZ. The magnitude of the SEMD drops to zero in the third BZ. The same pattern can be seen in the ΓM direction where the SEMD follows continuously bands σ_1, σ_2 and σ_3 and dies out in the third BZ. In the perpendicular ΓA direction there is almost no dispersion both in σ and π bands. Because of the asymmetry of the elementary cell the BZ is much narrower in the ΓA direction and the SEMD goes through approximately ten zones before it completely disappears.

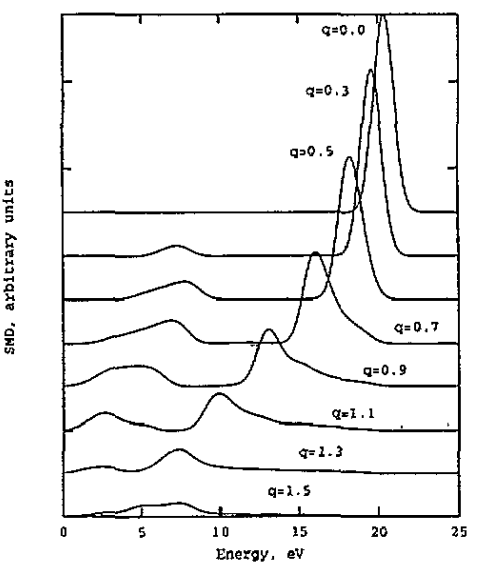

Figure 2. Spherically averaged spectral momentum density in graphite as a function of energy at constant momenta. Energy is relative to the Fermi level.

The spherically averaged SEMD $\rho_j(\epsilon, q)$ of equation (3) is plotted in figure 2 as a series of energy profiles at different momenta. One can see two main features in the plot. Their peak positions and integral intensities are plotted in column 4 of figure 1. The strongest peak originates from the σ bands and disperses like a free-electron parabola. The second weaker peak is the π band contribution. It shows little dispersion and has zero intensity at

$q = 0$. This behaviour has an obvious explanation. In the spherical average the areas close to the basal plane have much more statistical weight than those near the c axis. Since the σ band contribution to the EMD is roughly the same in all directions the spherical average will be close to the pattern seen in the basal plane, i.e. an average of the ΓM and ΓK directions. The π bands have maximum contribution to the EMD from the areas close to the c axis. After weighting with the statistical factor this results in a rather weak dispersion which is intermediate between the parabola-like dispersion in the ΓK and ΓM directions and lack of dispersion in the ΓA direction. The same can be said about the intensity of the π band.

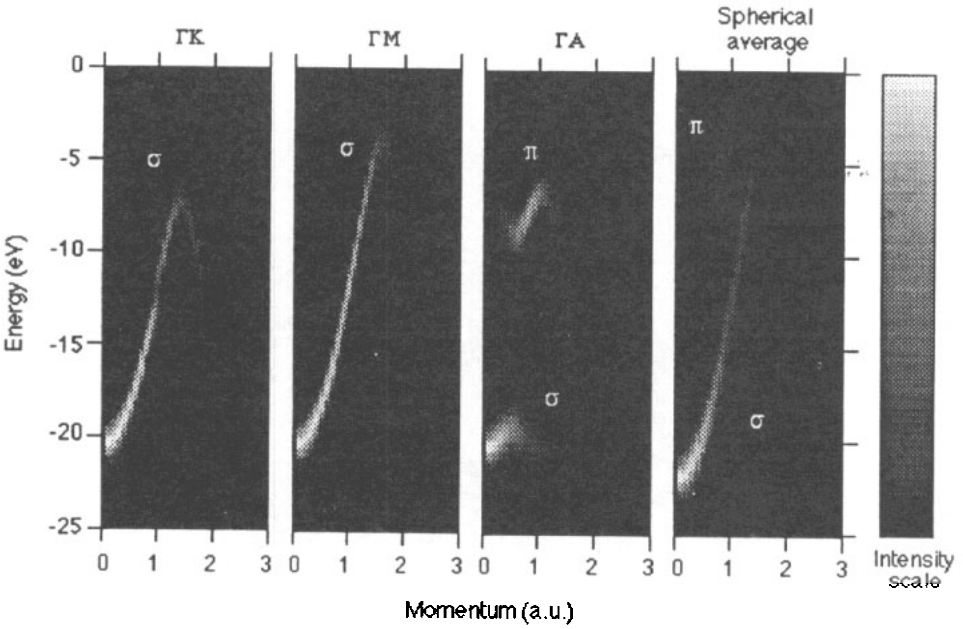

Figure 3. Linear grey scale plot of the SEMD $\rho_j(\epsilon, q)$ as a function of energy and momentum in ΓK, ΓM and ΓA directions and as a spherical average. Lighter shading represents greater intensity.

These characteristic features of the directional and spherically averaged SEMD are most clearly visible in figure 3 where it is plotted with a linear grey scale. To simulate a finite experimental energy resolution the theoretical curves are convoluted with a Gaussian corresponding to the FWHM = 1.5 eV. One can see a parabola-like dispersion in the σ band ΓK and ΓM directions as well as dispersionless π bands in the ΓA direction. The spherical average retains the parabolic dispersion of the σ bands. The most intense part of the π bands has also a similar type of dispersion.

At the present moment no high-resolution experimental data on fully oriented crystalline graphite samples have been reported. So we cannot test our results on directional momentum densities. However, we can validate our calculations by comparison to the experimental (e, 2e) data on the carbon samples.

These samples were prepared by laser annealing of amorphous carbon. This resulted in recrystallized films with a c axis perpendicular to the surface, but no ordering in the other direction, i.e. similar to HOPG. After transfer into vacuum (1×10^{-10} Torr) the samples were thermally annealed ($\simeq$600 °C) in order to clean the surface. For an unknown reason, these samples show significantly less intensity in between dispersing bands than conventional HOPG samples thinned by plasma etching. This could be due to remaining defects (i.e.

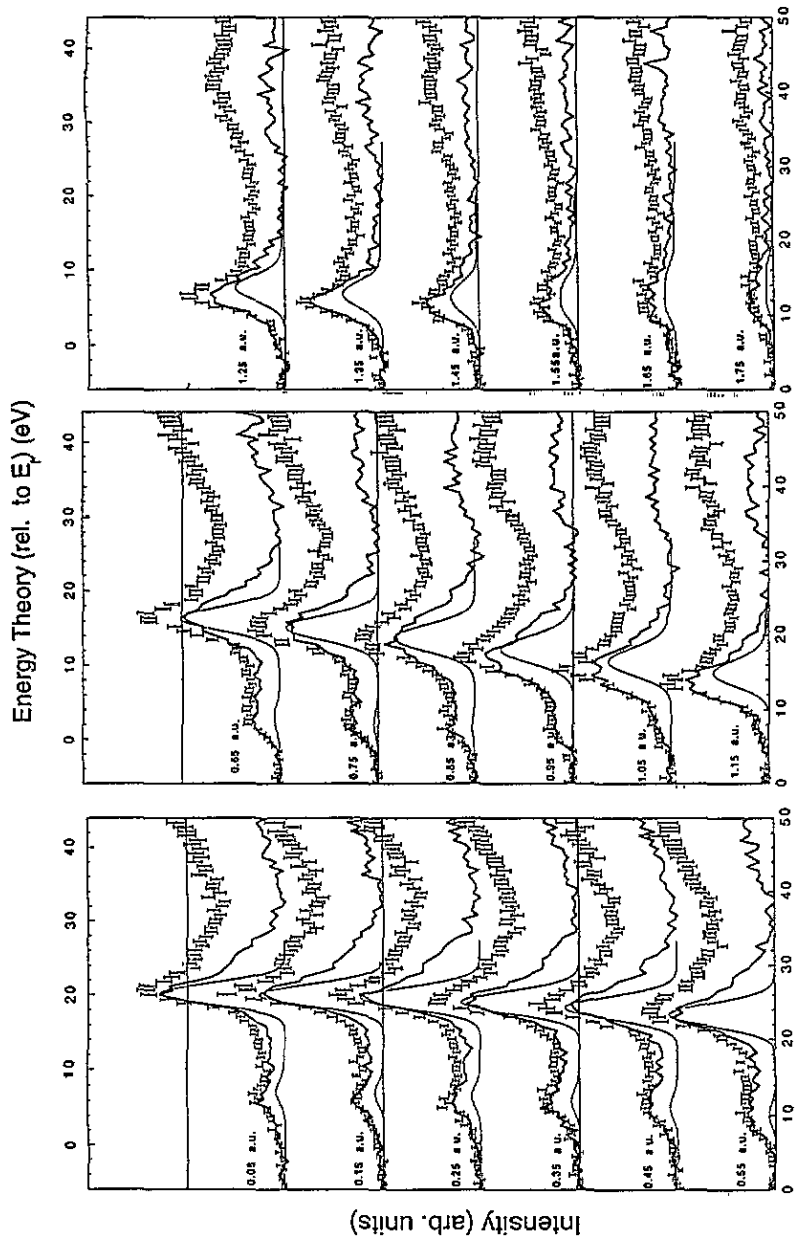

Figure 4. The experimental (e, 2e) spectra (error bars) for the different momenta perpendicular to the c axis as indicated. An attempt is made to correct for the inelastic energy loss contribution by plasmon excitation (thick solid line). The calculated spectra convoluted with an energy spread of 3 eV and momentum spread of 0.15 au are plotted as a thin solid line.

carbon vacancies) after plasma etching in the latter case. For further experimental details see Vos *et al* (1994) and Storer *et al* (1994).

In figure 4 we compare calculated energy profiles at various momenta with experimental data on laser-annealed carbon samples. Only the polar integration was carried out in the spherical average of equation (8) to simulate in-plane disorientation. In the experiment the momentum was kept perpendicular to the c axis, i.e. in the basal plane. However, because of the finite momentum resolution, there was a possibility for a finite out-of-plane component. We simulate this in our calculation by allowing a small fixed q_z component of 0.15 au. The experimental spectra in figure 4 are shown before and after deconvolution, a procedure which was designed to correct for plasmon energy loss contributions (Jones and Ritter 1986).

The two main features, σ and π, are reproduced well in our calculation. There is a shoulder in the lower-energy part of the experimental spectra which is absent in our calculation. This could be a contribution from the oxygen absorbed on the graphite surface. There is also a tail at high binding energies in the experiment. This could be due to the plasmon contribution which was not totally subtracted by the deconvolution procedure. It could also be correlational satellites which are common in atomic and molecular (e, 2e) spectra. A detailed discussion of these hypotheses goes beyond the scope of the present article.

4. Conclusion

We use the LMTO method to calculate the energy bands and momentum densities in high-symmetry directions in graphite and as the spherical average over the irreducible wedge of the Brillouin zone. The band energies are quite close to other theoretical and experimental results. Considerable improvement is achieved on the previous computation of Kheifets *et al* (1994) by adding empty spheres to the LMTO basis. The momentum densities resemble the calculations of Gao *et al* (1988) but a certain disagreement exists largely for in-plane ΓK and ΓM directions. High-resolution (e, 2e) experiments on oriented crystalline graphite targets are desirable to explain this difference.

Comparison of our in-plane averaged results with the experimental data on laser-annealed carbon indicates that the theory is valid for description of the major σ and π peaks. An explanation of the additional features seen in the experimental spectra requires going beyond the frame of the present model.

Acknowledgments

The authors wish to thank Professor H Skriver of the Technical University of Denmark for his heuristic arguments in applying the LMTO method to graphite. The laser-annealed carbon samples were kindly supplied by Professor F Bell of the University of Münich, Germany. This work is supported by an Australian Research Council grant.

References

Charlier J C, Gonze X and Michenaud J P 1991 *Phys. Rev.* B **43** 4579–89
Eberhardt W, McGovern J T, Plummer E W and Fischer J E 1990 *Phys. Rev. Lett.* **44** 200
Gao C, Ritter A L, Dennison J R and Holzwarth N A W 1988 *Phys. Rev.* B **37** 3914
Glötzel D, Segall R and Andersen O K 1980 *Solid State Commun.* **36** 403–6
Jones R and Ritter A 1986 *J. Electron Spectrosc. Relat. Phenom.* **40** 285

Kheifets A S, Lower J, Nygaard K, Utteridge S, Vos M, Weigold E and Ritter A L 1994 *Phys. Rev.* B **49** 2113–20
Kohn W and Sham L J 1965 *Phys. Rev.* **140** A1133
Law A R, Barry J J and Hughes H P 1983 *Phys. Rev.* B **28** 5332
McCarthy I E and Weigold E 1988 *Rep. Prog. Phys.* **51** 299
——1991 *Rep. Prog. Phys.* **54** 789
Skriver H L 1984 *The LMTO method* (Berlin: Springer)
Storer P, Caprari R S, Clark S A, Vos M and Weigold E 1994 *Rev. Sci. Instrum.* **65** 2214
Vos M, Storer P, Canney S, Kheifets A S, McCarthy I E and Weigold E 1994 *Phys. Rev.* B **50** 8
Wyckoff R 1963 *Crystal Structures* (New York: Interscience)